Nanoscale

Size-dependent Dislocation-twin Interactions

Journal:	*Nanoscale*
Manuscript ID	NR-ART-04-2019-003637.R1
Article Type:	Paper
Date Submitted by the Author:	12-Jun-2019
Complete List of Authors:	Wang, Jiangwei ; zhejiang univerisity, Materials Science and Engineering Cao, Guang; zhejiang univerisity, Materials Science and Engineering Zhang, Ze; Zhejiang University, Department of Materials Science and Engineering Sansoz, Frederic; The University of Vermont, School of Engineering

Size-dependent Dislocation-twin Interactions

Jiangwei Wang[1]*, Guang Cao[1], Ze Zhang[1], Frederic Sansoz[2]*

[1]Center of Electron Microscopy and State Key Laboratory of Silicon Materials, School of Materials Science and Engineering, Zhejiang University, Hangzhou 310027, China

[2]Department of Mechanical Engineering and Materials Science Program, The University of Vermont, Burlington, Vermont 05405, USA

*To whom correspondence should be addressed: jiangwei_wang@zju.edu.cn; frederic.sansoz@uvm.edu

Abstract

Dislocation-twin interactions critically control the plastic deformation and ultrahigh strength of nanotwinned metals. Here, we report a strong twin-thickness dependence of dislocation-twin interaction mechanisms from the tensile deformation of face-centered cubic metallic nanocrystals by *in situ* nanomechanical testing. Direct observations at atomic scale reveal that the predominant dislocation-twin interaction abruptly changes from dislocation transmission on the {111} slip planes to the unusual (100) slip plane of the twin, when the twin thickness is smaller than 4 layers. Using atomistic simulations, we find that the energy barrier for {100} slip transmission mechanism gradually decreases, with decreasing twin thickness, below the energy level required for normal (111) slip transmission, which remains identical for all twin sizes. Our *in situ* observations and simulations provide atomistic insights into a fundamentally new mechanism of plasticity in nanotwinned metals, down to the lowest twin size limit.

Dislocation-twin interactions play a fundamental role in the strengthening, plastic deformation, work-hardening and softening of bulk metals and metallic nanocrystals containing nanoscale coherent twin boundaries (TBs)[1-12]. In nanotwinned face-centered cubic (FCC) metals, an individual TB can act as a strong barrier for dislocation motion and nucleation[2,3,5,13], as well as an effective source for dislocation multiplication[10,14]. When a lattice dislocation is transmitted across a coherent TB, as schematically illustrated in Fig. 1a, dislocation dissociation generally occurs onto the (111) twin plane and the $(1\bar{1}\bar{1})_T$ plane, *i.e.* representing a mirror image of the $(1\bar{1}\bar{1})$ plane in the twin[14-17]. Thus far, all experimental evidence[5,12,14,15,17,18] indicates that the dislocation-twin interactions involve only {111} planes (either the (111) twin plane or the inclined $(1\bar{1}\bar{1})_T$ plane), primarily due to the high lattice resistance for dislocation slip on non-{111} planes in FCC metals at room temperature[16]. Theoretically, another possible scenario could be that slip on the {100} plane family in FCC metals becomes active because an incoming dislocation may not have enough time to adjust its slip plane in crossing a coherent TB, especially in nanosized crystals with ultrahigh stress, and because slip on the $(100)_T$ plane is geometrically favored when the loading orientation gives rise to a large Schmid factor on {100} planes, such as <111> loading[16]. (Note that $(100)_T$ plane is part of the {100} family). Furthermore, slip transmission on the $(100)_T$ plane has been simulated in nanotwinned Au crystals deformed at high strain rate by molecular dynamics (MD)[3,6,16,19-22]. However, it had never been observed experimentally under normal loading conditions.

Here, dislocation-twin interactions in different twinned Au nanojunctions have been investigated by using *in situ* nanomechanical testing conducted under high

resolution transmission electron microscopy (HRTEM) and MD simulations. We observe that the twin thickness strongly influences the dislocation transmission mechanism across the TB, which has been unknown in the literature. Namely, dislocation-twin interaction is dominated by slip on $(1\bar{1}\bar{1})_T$ planes when the twin thickness is large, whereas slip on the $(100)_T$ plane becomes predominant if the twin thickness is reduced to the angstrom scale. Therefore, our *in situ* experiments and atomistic simulation results should have important implications for understanding twin-thickness dependent plastic deformation and strengthening in nanotwinned metals approaching the smallest twin size limit.

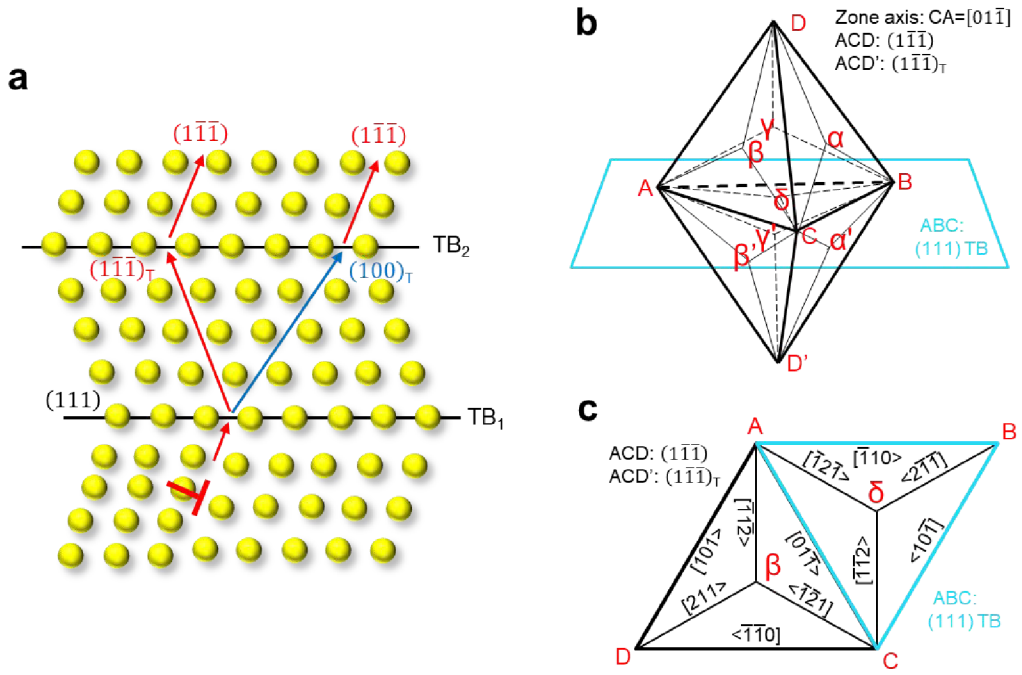

Figure 1. Standard and less common dislocation transmission mechanisms through a nanoscale twin in FCC metals. (a) Ordinary interaction on {111}-only slip planes frequently observed in experiments and simulations. In this case, dislocation DC = ½ [110] passes through a coherent TB and cross-slips onto the $(1\bar{1}\bar{1})_T$ plane at the first interface TB_1. However, dislocation-twin transmission on the $(100)_T$ plane is also possible theoretically, but rarely evidenced experimentally. **(b)** A double Thompson tetrahedron schematically showing the crystal slip orientation in nanotwinned FCC metals, where the ABC plane represents the TB plane. **(c)** Two-dimensional representation of the Thompson tetrahedron illustrating the possible slip planes and Burgers vectors of dislocations on the $(1\bar{1}\bar{1})$, $(1\bar{1}\bar{1})_T$ and (111) planes.

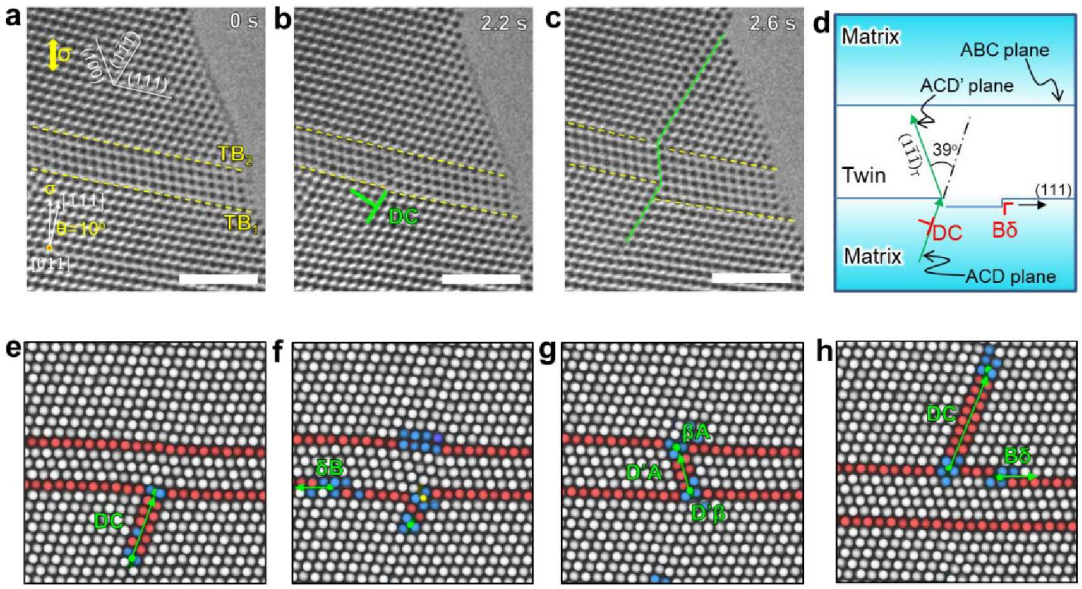

Figure 2. Classical {111}-only dislocation transmission through a perfect 4-layer twin in an Au nanojunction. (a-c) *In situ* HRTEM experimental evidence of {111} slip transmission. The nanojunction has a diameter of ~ 10 nm. The zone axis is $[01\bar{1}]$. All scale bars: 2nm. **(d)** Schematic illustration of the dislocation dynamics at the first TB interface. Upon deformation, a perfect 60° dislocation (*DC*) reacts with TB_1 and cross-slips onto the $(1\,\bar{1}\,\bar{1})_T$ and (111) twin planes. **(e-h)** A sequence of MD simulation snapshots showing each step of the transmission of dislocation *DC* through the interfaces TB_1 and TB_2. Coherent TB atoms are colored in red and uncoordinated atoms in blue. Dislocation extraction analysis (DXA) is superimposed to the deformed atomistic model, where the lines of Shockley partial and stair-rod dislocations are colored in green and yellow colors, respectively.

Fig. 2a-c presents direct *in situ* snapshots of a dislocation-TB interaction process observed during the straining of an Au nanojunction containing a single twin. The loading condition with respect to the nanojunction is indicated in Fig. 2a. Before deformation, the nanojunction is comprised of a 4-layer twin made of two perfectly coherent TBs separated by 0.94 nm. Here, the number of twin layers corresponds to the number of {111} interplanar spacings in the thickness between the two coherent TBs. A double Thompson tetrahedron and its two-dimensional representation are schematically represented in Figs. 1b and 1c, respectively, to help understand the dislocation dynamics and slip vectors for transmission across the (111) twin plane.

Upon tension, a perfect 60° dislocation (*DC*) is emitted from the free surface, glides on the *ACD* plane, and is blocked by the first interface, TB_1 (*ABC* plane), as shown in Fig. 2b. This observation agrees with the well-accepted conclusion that coherent TBs are strong barriers for dislocation motion[1,4,5,12]. The interaction between the incoming dislocation and TB_1 results in a slight incoherent kink-like step on the coherent interface. After further straining, the dislocation transmits across both TB_1 and TB_2 by dissociating and cross-slipping onto the $(1\,\bar{1}\,\bar{1})_T$ plane, Fig. 2c. Accompanying this process is the enlargement of the step on TB_1 and the thickening of the righthand side of the twin by one layer (increased to 5 layers), due to the transverse slip of a twinning partial $B\delta$ on TB_1, as schematically illustrated in Fig. 2d.

Evidently, the above dislocation-twin interaction exhibits the standard {111} slip mechanism[5,12,14,15,18,23]; however, determining the exact dislocation dynamics at the interfaces remains technologically challenging due to the high dislocation velocity. Therefore, we used MD simulations to systematically study the interaction of a perfect dislocation *DC* with a 4-layer twin under applied stress (see *Methods* for details). Atomistic deformation snapshots in Figs. 2e-h and Movie S1 reveal all important steps involved in the transmission of dislocation *DC* through both TB_1 and TB_2. DXA analysis allowed us to obtain a detailed sequence of dislocation reactions during transmission as follows. First, all evidence from simulation (Fig. 2e) and experiments (Fig. 2b) indicate that the perfect dislocation *DC* is constricted before reaction with TB_1, then dissociates on the (111) TB plane such as:

$$DC \rightarrow D\delta + \delta C \tag{1}$$

where $D\delta$ is equivalent to $\delta D'$ (hereafter, a prime is used only for dislocations emitted inside the twin). Therefore, it further dissociates to emit a perfect dislocation into the twin:

$$D\delta \rightarrow \delta D' \rightarrow AD' + \delta A \quad (2)$$

Also, given that from Fig. 1c,

$$\delta A + \delta C = B\delta \quad (3)$$

Substituting (2) and (3) into (1) yields the first reaction at TB_1 to be consistent with the experimental observation in Figs. 2c,d:

$$DC \rightarrow AD' + B\delta \ \text{(at } TB_1\text{)} \quad (4)$$

This reaction produces a twinning partial dislocation $B\delta$, which propagates on the (111) TB plane and increases the twin thickness by 1 layer. Furthermore, another possible mechanism is that the perfect dislocation *DC* constricts to produce *CD*, and then reacts at TB_1 according to

$$CD \rightarrow D'A + \delta B \ \text{(at } TB_1\text{)}, \quad (5)$$

which is in better agreement with the MD simulation snapshot presented in Fig. 2f. Following (5), or equivalently (4), the perfect dislocation *D'A* dissociates into a leading 30^o partial dislocation and a trailing 90^o partial, leaving behind a stacking fault (SF) between the two TBs, as evidenced experimentally by the lattice kink in Fig. 2c and in MD simulation in Fig. 2g:

$$D'A \rightarrow D'\beta + \beta A \quad (6)$$

When *D'A* reaches the second twin plane TB_2, it cross-slips again on the twin plane:

$$D'A \rightarrow D'\delta + \delta A \ , \quad (7)$$

followed by emission of a constricted perfect dislocation *DC* into the upper matrix according to the reaction,

$$D'\delta \rightarrow \delta D \rightarrow CD + \delta C \rightarrow DC + \delta C \quad (8)$$

Substituting (8) and (3) into (7) yields the second reaction at TB_2:

$$AD' \rightarrow DC + B\delta \text{ (at } TB_2\text{)} \quad (9)$$

Another twinning partial dislocation $B\delta$ propagates along TB_2 in the opposite direction to the twinning partial moving on TB_1, which increases the entire twin thickness by one layer as shown in Fig. 2h. Therefore, the above reaction sequence suggests that the experimental snapshot showing the zigzag slip lines in Fig. 2c is at an intermediate state between the MD simulation images in Fig. 2g and Fig. 2h, because only half of the initial 4-layer twin has been transformed into a 5-layer one. Overall, these dislocation reactions are consistent with the dislocation-twin interaction mechanisms frequently observed in previous studies[1,4,5,12,15,16,18].

Remarkably, the dislocation-twin interaction exhibits a pronounced change in behavior when the twin thickness is reduced to its minimum limit at the angstrom scale. Fig. 3 presents an example of previously unexpected dislocation-twin interaction in an Au nanojunction containing a 2-layer twin (the minimum twin thickness in FCC metals). This sample is subjected to the same loading condition as that in Fig. 2a-c. Initially, the Au nanojunction has a coherent twin structure with no lattice imperfection. Upon deformation, a perfect dislocation (denoted as DC_1) is emitted from the free surface, then propagates towards the nanojunction, and is blocked by the first coherent twin interface TB_1, Fig. 3a. However, further loading induces an uncommon dislocation-twin interaction mechanism associated with the transmission of DC_1 across the whole 2-layer twin, Fig. 3b. Surprisingly, although DC_1 glides onto the $(1\bar{1}\bar{1})$ plane of the upper matrix after traversing the 2-layer twin, its slip geometry suggests that it may pass through the

twin by cross-slipping onto the unconventional $(100)_T$ plane, as marked out by the purple line in Fig. 3b, leaving two parallel TB ledges behind. Subsequently, it appears in Fig. 3c that one TB ledge has migrated away towards the free surface, which increased the twin thickness by one more layer. At the same time, a second perfect dislocation DC_2 is emitted from the surface and reacts with TB_1 in the same manner as identified based on the slip geometry, thereby contributing to the formation of a perfect 4-layers twin, Fig. 2d.

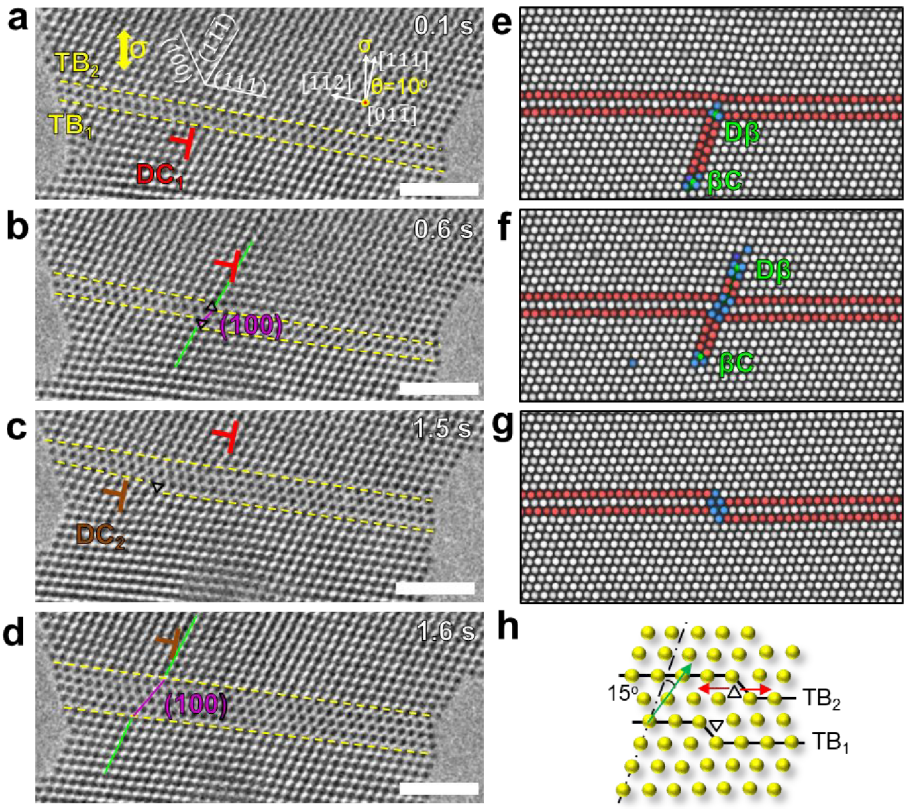

Figure 3. Unusual dislocation-twin interaction on the $(100)_T$ plane in a pristine Au nanojunction containing a perfect 2-layer twin. The diameter of the nanojunction is about 9.5 nm. **(a)** Upon deformation, a full dislocation DC_1 is emitted from the free surface and blocked by TB_1. The loading orientation is the same as that in Fig. 2a. **(b)** Further loading induces direct transmission of DC_1 across the 2-layer twin. Associated with dislocation transmission is the formation of two parallel TB ledges, the migration of which results in twin thickening from 2 to 3 layers. **(c-d)** A second dislocation DC_2 is emitted and reacts with the twin in the same manner, resulting in a total transformation to a 4-layer twin. All scale bars: 2 nm. **(e-g)** MD simulation snapshots of dislocation transmission through a 2-layer twin. **(h)** Atomic structure of two TB ledges (triangles) formed after $(100)_T$ slip transmission. The semi-coherent ledges migrate parallel to the twin plane under stress.

MD simulation was also used to study the reaction details from the above example, because it could not be directly capture *in situ* due to the small twin thickness and ultrafast dislocation propagation process. Fig. 3e-f and Movie S2 reveal the full transmission of perfect dislocation *DC* across the 2-layer twin, after constriction at TB_1, such as:

$$\frac{1}{2}(1\bar{1}\bar{1})[110] \rightarrow \frac{1}{2}(100)_T[011]_T \quad (10)$$

or also

$$DC \rightarrow D'B \text{ (at } TB_1) \quad (11)$$

and then reciprocally,

$$D'B \rightarrow DC \text{ (at } TB_2) \quad (12)$$

Here, the (100) dislocation *D'B* is consistent with that found by previous MD simulations from Ezaz *et al.*[16] It is also important to note that the twin thickness is smaller than the length of the stacking-fault ribbon connecting the leading and trailing partial dislocations, which resulted in the stacking-fault cutting entirely through the twin as shown in Fig. 3f. Nevertheless, all dislocations involved in reactions (10)-(12) unexpectedly cross-slip onto the $(100)_T$ plane only. Furthermore, our DXA analysis in Fig. 3g suggests that the two TB ledges left behind after reaction are not twinning partial dislocations like those formed during {111} slip transmission but rather are FCC disclinations on a perfectly coherent interface as schematically illustrated in Fig. 3h. These semi-coherent disclinations can move easily along the TB planes under an applied stress, resulting in either thickening or thinning of the pre-existing twin by one layer, as indicated by the thickness increase of the righthand side of the twin from 2 layers to 3 layers in Fig. 3d.

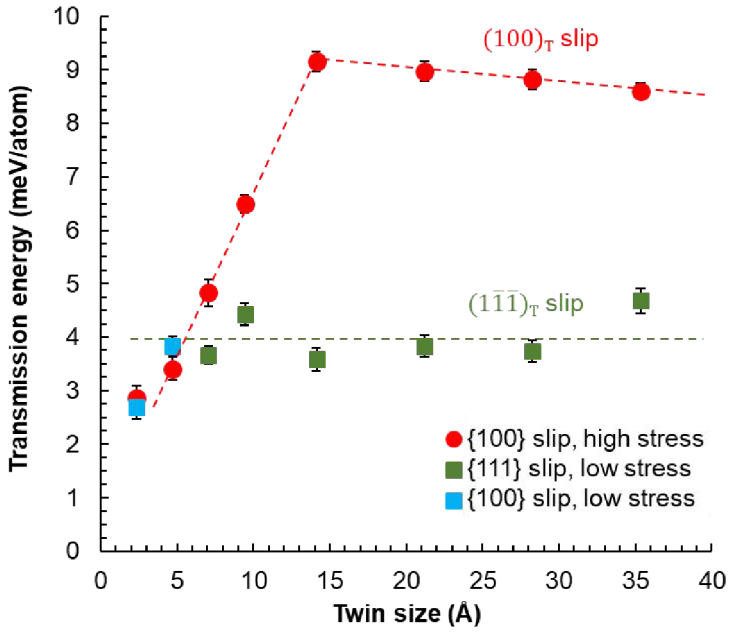

Figure 4. Twin-size dependence of the energy barrier for dislocation transmission through the first TB_1 interface for either $(1\bar{1}\bar{1})_T$ or $(100)_T$ slip mechanisms predicted by MD simulations. Low loading-stress configuration was simulated using free low-energy {111} surfaces and deformation imposed by stress intensity from a pile-up of 3 dislocations, while high loading-stress configuration was simulated using an infinitely large junction with periodic boundaries, and deformation imposed by uniform tension. Here, the number of twin layers corresponds to the number of {111} interplanar spacings in the thickness between the two coherent TBs.

To compare different dislocation-twin interaction mechanisms in FCC metals, previous studies have used classical continuum theory to estimate for the energy barrier for dislocation transmission through a single coherent TB[13]. This methodology, however, neglects both non-{111} slip mechanisms and twin-size effects. Therefore, we have conducted a series of MD simulations to calculate the twin-size dependence of the transmission energy barrier for nanoscale twins of different thicknesses, Fig. 4 (See *Methods* for details). It is worth mentioning that we have considered two types of loading

conditions on the nanojunction, both low- and high-loading stresses, because the occurrence of {100} slip transfer has been shown to require high stresses and high strain-rates in past simulation studies[3,6,16,21,22]. In the present simulations, we systematically find the $(100)_T$ slip transmission mechanism under high local stresses, when the crystal is modeled without free surfaces using periodic boundary conditions, and deformed under uniform tension. On the contrary, we find either {111} or {100} slip mechanisms under low local stresses that are achieved by simulating the crystal with free boundaries using only {111} surface facets, and localized stress intensity resulting from dislocation pile-up deformation.

From Fig. 4, our MD simulations predict that the energy barrier associated with transmission on the $(1\bar{1}\bar{1})_T$ slip plane remains quasi-constant for all twin thicknesses studied. In stark contrast, the highest energy barrier for slip transmission on $(100)_T$ is for twin thickness larger than 1.4 nm, or 6 twin layers, and then decreases dramatically when reduced below this limit. Consequently, we discover that the energy barrier for $(100)_T$ slip transmission mechanism gradually decreases with decreasing twin thickness, below the energy level required for normal $(1\bar{1}\bar{1})_T$ slip transmission, at about 0.7 nm or 3 layers. In fact, Fig. 4 indicates that only $(100)_T$ slip mechanism occurs for both low and high loading stress configurations below a transition threshold of 3 layers.

To further validate the size-dependent dislocation-twin interaction, two additional Au nanojunctions with twins of different thicknesses were studied, Fig. 5. The first as-fabricated Au nanojunction contained two neighboring twins of 3 and 7 layers in thickness, respectively. Upon deformation, a 90° leading partial $D\beta$ and a SF are emitted sequentially from a surface step, first interact with TB_1, and then traverse the 3-layer twin,

Fig. 5a-c. HRTEM observation further confirms that the dislocation transmission process through the 3-layer twin occurred on the $(100)_T$ plane, as evidenced by the zoomed-in image of a SF-like lattice kink on the $(100)_T$ plane in Fig. 5d. Further deformation induces the nucleation of a 30° trailing partial βC from the same surface site, which propagates along the pathway of the leading partial, causing the annihilation of the SF and the formation of a full dislocation DC at TB_3, Fig. 5c. Similarly, dislocation transmission on $(100)_T$ plane has left a TB ledge on TB_2. This *in situ* observation is consistent with our MD simulation result predicting only $(100)_T$ slip transition at a twin of 3 layers.

Furthermore, the interaction between two individual SFs further confirms the conclusion that dislocation can slip on $(100)_T$ plane if the twin thickness is small. Fig. 5e-g shows that two SFs nucleate sequentially from the free surface under deformation and interacts with each other inside the crystal by forming a SF intersection. A zoomed-in image in Fig. 5g indicates that the intersection between SF_1 and SF_2 occurs along the direction of $(100)_T$ plane (indicated by the green dashed line), similar to the dislocation-twin interaction found experimentally in Fig. 3 and Fig. 5a-d, and in good agreement with the atomistic configuration leading to the lowest energy barrier in MD prediction in Fig. 4. Collectively, these results unequivocally prove that the twin-dislocation interaction mechanism is strongly twin-size dependent.

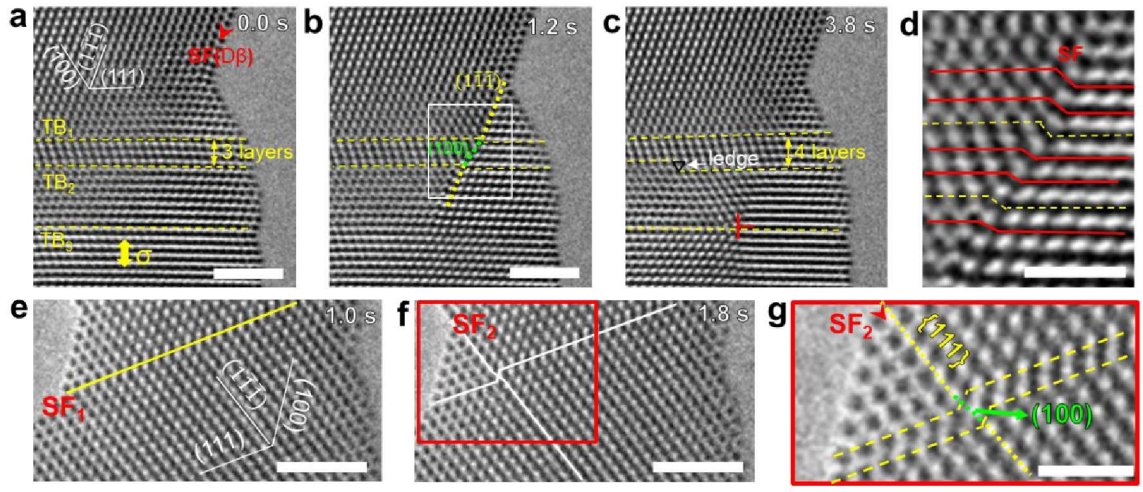

Figure 5. Examples of dislocation-twin interaction on the $(100)_T$ plane in other twinned or stacking-faulted Au nanojunctions. (a) As-fabricated Au nanojunction containing two neighboring twins with the size of 3-layers and 7-layers, respectively. The diameter of the nanojunction is ~8 nm. **(b)** Upon deformation, a *Dβ* leading partial nucleates from the free surface, leaving a stacking-fault (SF) behind, interacts with twin interface TB_1 and traverses the 3-layer twin. **(c)** Successive nucleation and propagation of the trailing partial induces the annihilation of the SF and recombines with the leading partial as a full dislocation at TB_3. A TB ledge left behind migrates to add one more layer to the twin. **(d)** Zoomed-in image of (b) showing a SF-like lattice kink on the $(100)_T$ plane of the 3-layer twin. **(e-g)** Interaction between two individual SFs. The diameter of the nanojunction is ~6 nm. Zoomed-in image in (g) showing that the intersection between SF_1 and SF_2 occurred along the direction of $(100)_T$ plane, as indicated by the green dashed line. Scale bars in (a-c) and (e-f) are 2 nm, and scale bars in (d) and (g) are 1 nm.

{100} planes are not close-packed in FCC metals, and thus the Peierls stress to activate {100} slip is much higher than that of ordinary {111} slip. For example, the energy barrier for the (100) slip is 1614 $mJ \cdot m^{-2}$ for copper, in stark contrast to the 167 $mJ \cdot m^{-2}$ for the slip of partial dislocations on $(\bar{1}\bar{1}\bar{1})$ planes[16]. Due to the high energy barrier of {100} slip, dislocation glide on {100} planes is energetically unstable and would generally dissociate quickly into partial dislocations on {111} planes[19,22]. However,

our experimental observations (Figs. 2, 3 and 5) and theoretical calculations (Fig. 4) clearly demonstrate that the conventional dislocation-twin interaction on the $(1\bar{1}\bar{1})_T$ plane would transfer on to the $(100)_T$ plane if the twin thickness is reduced to the angstrom scale. The occurrence of this unexpected dislocation dynamics should be helped by the ultrahigh applied stress and ultrathin twin thickness. For instance, it was observed that angstrom scale twins can harden nanotwinned metals significantly, resulting in a near-ideal theoretical strength[11,24].

Table 1. Schmid factors of dislocations transmitted onto different slip planes of the twin in this study

Samples	Twin thickness	Dislocation Type	Burgers vector	Schmid factor	Active slip planes
Fig. 2a-c	4 layers	D'A	$\frac{1}{2}(1\bar{1}\bar{1})_T[101]_T$	0.148	$(1\bar{1}\bar{1})_T$
		D'B	$\frac{1}{2}(100)_T[011]_T$	0.500	
Fig. 3	2 layers	D'A	$\frac{1}{2}(1\bar{1}\bar{1})_T[101]_T$	0.148	$(100)_T$
		D'B	$\frac{1}{2}(100)_T[011]_T$	0.500	
Fig. 5a-d	3 layers	D'A	$\frac{1}{2}(1\bar{1}\bar{1})_T[101]_T$	0.254	$(100)_T$
		D'B	$\frac{1}{2}(100)_T[011]_T$	0.471	

A past study also suggested that the loading orientation could influence dislocation-twin interactions to some extent since the critical resolved shear stress on the slipping planes changes with the loading orientation[16]. In the examples presented in our studies, the $(100)_T$ planes possessed much higher Schmid factors than the $(1\bar{1}\bar{1})_T$ plane (Table 1). Given the ultrahigh strength and high critical resolved shear stress in

nanotwinned Au samples, the slip on the $(100)_T$ plane may be activated even though it has an ultrahigh high energy barrier[16]. Besides, for angstrom-scale twins, the overall energy rise induced by the dislocation slip on the $(100)_T$ plane can be considered negligible under high stress, as predicted by MD in Fig. 4. As a result, an incident dislocation could more easily cut the twin along the $(100)_T$ plane, rather than along the conventional $(1\bar{1}\bar{1})_T$ slip. However, the energy required for the slip transmission of the twin on $(100)_T$ slip increases markedly with the twin thickness, resulting in strong twin-size dependent twin-dislocation interaction. In other words, $(100)_T$ slip in nanotwinned metals should only occur in the case when the twin thickness is rather small. Our present results support this hypothesis.

During dislocation-twin interaction in samples with ultrathin twins, an incident partial/full dislocation can pass through the TB by cross-slipping onto the $(100)_T$ plane[21] following reactions (10)-(12). During transmission inside the twin, however, the newly formed dislocation segment usually adopts an arc shape since the two ends of the embossed dislocation segment are pinned on the TB. According to a previous study[21], the maximum radius of the dislocation segment, *i.e.* the largest curved dislocation segment that can stably exist on the $(100)_T$ plane before the occurrence of its dissociation, can be expressed as: $r_c = \alpha\mu b/\sigma_c$, where r_c is the curvature of the dislocation segment, μ is the shear modulus, b is the Burgers vector of the dislocation, σ_c is the applied resolved shear stress on the $(100)_T$ plane, $\alpha \approx 0.5$. For Au, $\mu = 20.9$ GPa[25], b = 0.2876 nm for a full dislocation on this slip plane. In Fig. 5, the estimated resolved shear stress on the $(100)_T$ plane is about 2.8 GPa (The maximum elastic lattice strain just before the dislocation nucleation is ~5.17% and the Young's modulus of single crystal Au along the [111]

direction is about 116 GPa[24]. The estimated resolved shear stress on the $(100)_T$ plane can be calculated by $\sigma = \varepsilon * G * m$, here m is the Schmid factor of dislocation slip on $(100)_T$ plane.), giving a critical twin thickness of $\lambda \approx 1$ nm, which is close to the thickness of a 3-layer twin in Au. This theory is consistent with our experimental and MD simulation observations.

In conclusion, we have discovered a strong twin-size dependence dislocation-twin interaction in FCC metallic nanocrystals using *in-situ* nanomechanical testing and MD simulations, associated with an unusual slip transmission on $(100)_T$ plane with angstrom-scale twins less than 4 layers (0.94 nm) in thickness. Given the higher energy barrier for $(100)_T$ slip transmission in FCC metals, such dislocation-twin interaction mechanism is expected to play an important role in the size-dependent strengthening and ductile-to-brittle transition behaviors of nanotwinned nanowires, especially at the minimum twin size limit[8,11,26].

Experimental Methods

In situ TEM nanomechanical testing

In situ tensile testing of nanotwinned Au nanocrystals was conducted inside a FEI Titan Cs-corrected TEM, equipped with a TEM-Scanning tunnelling microscope (STM) holder from Beijing PicoFemto Co. Before tension experiments, nanotwinned Au nanocrystals were fabricated inside the TEM by welding two Au rods together under a voltage potential[27,28]. In a typical experiment, a bulk Au rod with numerous nanoscale tips on the fracture surface was loaded onto the static side of the TEM holder; while, an Au probe on the other end of the TEM holder was used to control the sample by a piezo-manipulator. Subsequently, the Au probe was manipulated to contact with a nanoscale tip on the Au rod at the static side of the holder, and nanotwinned Au nanojunctions were fabricated by welding the Au probe and the nanoscale tips together under a voltage

potential of ~1V. Then, the nanotwinned Au nanocrystals were loaded along their axial direction at a constant rate of ~0.005 nm/s, which resulted in an estimated strain rate of 10^{-3} s^{-1}. All *in situ* experiments were conducted under HRTEM and weak beam conditions. Dynamic structural evolutions of nanotwinned Au nanocrystals were recorded in real time by a CCD camera at a rate of ~0.3 s/frame.

Simulation Methods

MD simulations were performed with the software LAMMPS[29] using an embedded-atom-method potential for gold developed by Grochola et al.[30]. This potential predicts a value of the stacking-fault energy for this metal (43.4 $mJ \cdot m^{-2}$) that is close to experimental data (32 ~ 46.4 $mJ \cdot m^{-2}$)[30]. Based on past MD studies[21], it is already known that dislocation transmission on (100} plane is very short-lived and only observed under high stress conditions typically encountered by MD. Therefore, in this study, we have simulated dislocation transmission on either $\{111\}_T$ or $(100)_T$ planes, by changing the type of loading stress applied to the twinned nanojunction, *low* or *high*, respectively. Twin-slip interaction under *low* loading-stress conditions was simulated using a nanoscale [111]-oriented bicrystal containing two coherent (111) TBs and free surfaces made of only low-energy {111} facets, as shown in Fig. S1a. The initial model dimensions were 24 nm × 27.4 nm × 4.6 nm. Deformation was simulated by continuously adding new edge dislocations of the *DC* type, to produce a dislocation pile-up generating a stress intensity at the dislocation-twin intersection. New dislocations were introduced by displacing one half of the bottom line of atoms at a constant velocity of 3 $m \cdot s^{-1}$, while keeping the other half at a fixed position. Twin-slip interaction under *high* loading-stress conditions was simulated using a semi-infinite [111]-oriented bicrystal containing only two coherent (111) TBs and two fixed surfaces on top and bottom sides, as shown in Fig. S1b. The initial model dimensions were 31.8 nm × 28.4 nm × 4.6 nm. Deformation was simulated by first adding 1 new edge dislocation of the *DC* type from the bottom side, using the above technique, followed by pure uniform tensile deformation along the y-axis at a constant velocity of 3 $m \cdot s^{-1}$. The twin spacing was varied from 1 layer (intrinsic stacking-fault) to 15 layers (3.5 nm). Periodic boundary conditions were imposed on the out-of-plane z-axis for all models. Simulations were carried out using a Verlet algorithm

with constant NPT integration with zero pressure along the z axis and a time step of 2 fs. Before deformation, the energy of each model was minimized by conjugate gradient method and relaxed at 300K for 50 ps under zero stress. Deformation was performed at 300K±0.5K.

ASSOCIATED CONTENT

AUTHOR INFORMATION

Corresponding Authors

*E-mail: J.W. (jiangwei_wang@zju.edu.cn); F.S. (frederic.sansoz@uvm.edu).

ORCID

Jiangwei Wang: 0000-0003-1191-0782

Frederic Sansoz: 0000-0002-2782-1832

Notes:

The authors declare no competing financial interest.

ACKNOWLEDGMENTS

J.W. acknowledges the support of the National Natural Science Foundation of China grants (Nos. 51771172 and 51701179) and the Innovation Fund of the Zhejiang Kechuang New Materials Research Institute (No. ZKN-18-Z02). F.S. received support for this research from U.S. Department of Energy grant no. DE-SC0016270. The simulations in this research used the resources of the Extreme Science and Engineering

Discovery Environment (XSEDE), supported by U.S. National Science Foundation grant No. ACI-1548562.

REFERENCES

1 Lu, L., Shen, Y. F., Chen, X. H., Qian, L. H. & Lu, K. *Science* (2004), **304**, 422-426.
2 Zhu, T., Li, J., Samanta, A., Kim, H. G. & Suresh, S. *Proceedings of the National Academy of Sciences* (2007), **104**, 3031-3036.
3 Afanasyev, K. A. & Sansoz, F. *Nano Letters* (2007), **7**, 2056-2062.
4 Lu, L., Chen, X., Huang, X. & Lu, K. *Science* (2009), **323**, 607-610.
5 Lu, K., Lu, L. & Suresh, S. *Science* (2009), **324**, 349-352.
6 Deng, C. & Sansoz, F. *Nano Letters* (2009), **9**, 1517-1522.
7 Li, X., Wei, Y., Lu, L., Lu, K. & Gao, H. *Nature* (2010), **464**, 877-880.
8 Jang, D., Li, X., Gao, H. & Greer, J. R. *Nat. Nanotechnol.* (2012), **7**, 594-601.
9 Zhu, T. & Gao, H. *Scripta Materialia* (2012), **66**, 843-848.
10 Wang, Y. M., Sansoz, F., LaGrange, T., Ott, R. T., Marian, J., Barbee Jr, T. W. & Hamza, A. V. *Nature Materials* (2013), **12**, 697-702.
11 Wang, J., Sansoz, F., Huang, J., Liu, Y., Sun, S., Zhang, Z. & Mao, S. X. *Nat. Commun.* (2013), **4**, 1742.
12 Sansoz, F., Lu, K., Zhu, T. & Misra, A. *MRS Bulletin* (2016), **41**, 292-297.
13 Zhu, Y. T., Wu, X. L., Liao, X. Z., Narayan, J., Kecskés, L. J. & Mathaudhu, S. N. *Acta Materialia* (2011), **59**, 812-821.
14 Li, N., Wang, J., Misra, A., Zhang, X., Huang, J. Y. & Hirth, J. P. *Acta Materialia* (2011), **59**, 5989-5996.
15 Wang, Y. B. & Sui, M. L. *Applied Physics Letters* (2009), **94**, 021909.
16 Ezaz, T., Sangid, M. D. & Sehitoglu, H. *Philosophical Magazine* (2011), **91**, 1464-1488.
17 Ni, S., Wang, Y. B., Liao, X. Z., Figueiredo, R. B., Li, H. Q., Ringer, S. P., Langdon, T. G. & Zhu, Y. T. *Acta Materialia* (2012), **60**, 3181-3189.
18 Wang, J. & Mao, S. X. *Extreme Mechanics Letters* (2016), **8**, 127-139.
19 Deng, C. & Sansoz, F. *Acta Materialia* (2009), **57**, 6090-6101.
20 Wang, J. & Huang, H. *Applied Physics Letters* (2006), **88**, 203112.
21 Wu, Z. X., Zhang, Y. W. & Srolovitz, D. J. *Acta Materialia* (2011), **59**, 6890-6900.
22 Wu, Z. X., Zhang, Y. W. & Srolovitz, D. J. *Acta Materialia* (2009), **57**, 4508-4518.
23 Cao, Y., Wang, Y. B., An, X. H., Liao, X. Z., Kawasaki, M., Ringer, S. P., Langdon, T. G. & Zhu, Y. T. *Scripta Materialia* (2015), **100**, 98-101.
24 Deng, C. & Sansoz, F. *ACS Nano* (2009), **3**, 3001-3008.
25 Ogata, S., Li, J., Hirosaki, N., Shibutani, Y. & Yip, S. *Physical Review B* (2004), **70**, 104104.
26 Wang, J., Sansoz, F., Deng, C., Xu, G., Han, G. & Mao, S. X. *Nano Letters* (2015), **15**, 3865-3870.
27 Wang, J., Zeng, Z., Weinberger, C. R., Zhang, Z., Zhu, T. & Mao, S. X. *Nat Mater* (2015), **14**, 594-600.
28 Zhu, Q., Cao, G., Wang, J., Deng, C., Li, J., Zhang, Z. & Mao, S. X. *Nature Communications* (2019), **10**, 156.
29 Plimpton, S. *Journal of Computational Physics* (1995), **117**, 1-19.

30 Grochola, G., Russo, S. P. & Snook, I. K. *The Journal of Chemical Physics* (2005), **123**, 204719.

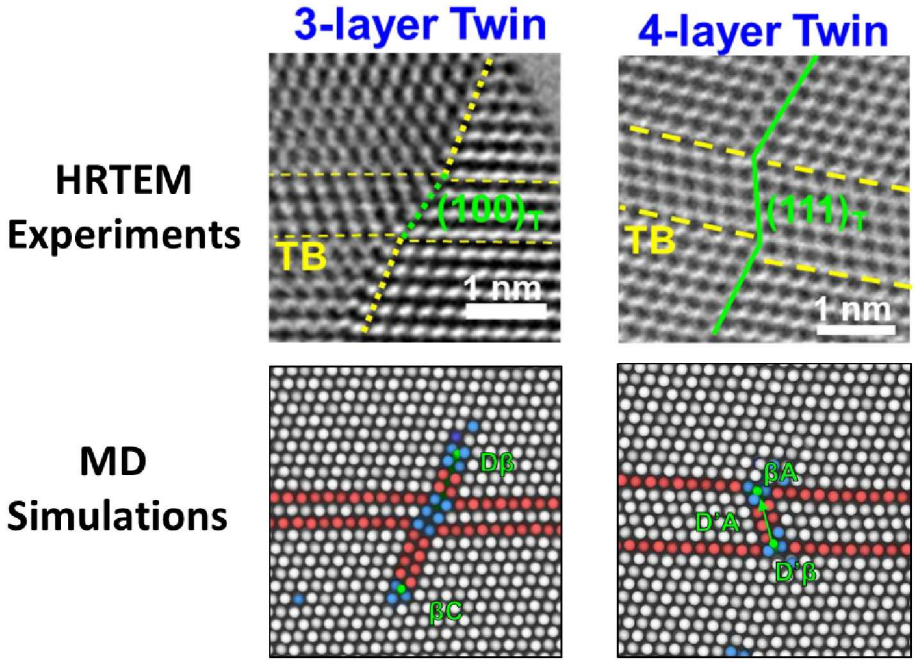

Dislocation-twin interaction show a strong twin size dependence down to the smallest twin size limit.